A novel inorganic Ni-La_2O_3 composite with superfast and versatile water purification behavior

Xing, Yan; Cheng, Jing; Zhang, Mengfei; Zhao, Meng; Ye, Liyan; Pan, Wei

DOI
10.1021/acsami.8b17114

Publication date
2018

Document Version
Final published version

Published in
ACS Applied Materials and Interfaces

ACS APPLIED MATERIALS & INTERFACES

Research Article

Cite This: ACS Appl. Mater. Interfaces 2018, 10, 43723−43729

www.acsami.org

A Novel Inorganic Ni−La_2O_3 Composite with Superfast and Versatile Water Purification Behavior

Yan Xing,[†] Jing Cheng,[†] Mengfei Zhang,[†] Meng Zhao,[‡] Liyan Ye,[§] and Wei Pan*[,†]

[†]State Key Laboratory of New Ceramic and Fine Processing, Department of Materials Science and Engineering, Tsinghua University, Beijing 100084, P. R. China

[‡]Department of Materials Science and Engineering, Delft University of Technology, Delft, The Netherlands

[§]Center for Clinicla Laboratory Medicine, PLA General Hospital, Beijing 100853, P. R. China

Supporting Information

ABSTRACT: Water-purifying materials are of vital importance for providing sanitary water, especially in epidemic and disaster areas and for wilderness survival. Here, we report a novel inorganic composite with a fast, reusable, and pleiotropic water purification ability. The composite of heterogeneous Ni−La_2O_3 nanofibers was developed using an easy, low-cost, and large-scale production process, i.e., an electrospinning technique. Because of the unique heterostructure formed by introducing nickel nanoparticles into the La_2O_3 host, the nanocomposite fibers can rapidly remove various detrimental micropollutants with absorption rate constants hundreds of times greater than those of inorganic materials and activated carbons. In addition, the nanocomposite can be recycled by a soft washing procedure at ambient temperature and demonstrates a much more stable performance than the state-of-the-art activated carbon materials. Furthermore, the nanofibers have an excellent germicidal effect against the high-risk human pathogen *Escherichia coli*. Our work introduces a promising inorganic absorbent suitable for purifying life-sustaining water supplies in emergency situations and alleviating worldwide water shortages.

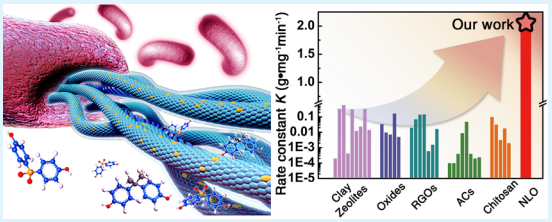

KEYWORDS: *ultrafast absorption, heterostructure, recovery, emerging contaminants removal, water disinfection*

1. INTRODUCTION

The contamination of water resources by micropollutants and microbes, which have long-term effects on human health or cause contagious diseases, has evolved into one of the most severe global issues in human society.[1−5] Such endocrine disrupting chemicals (EDCs), a series of typical organic micropollutants, are nonbiodegrade and acutely toxic to the living organism even under low concentration.[6,7] Microbes are another kind of harmful pollutant thriving in wastewater, which can also cause different types of detrimental diseases. Thus, a method to quickly remove these water contaminants and conveniently provide sanitary water is needed.

Absorption is considered as the best and most universal technique for micropollutants removal, and various absorbents have been reported.[8] Among them, activated carbon materials are currently most widely used to remove organic pollutants from wastewater. However, the relatively low absorption rates, high regeneration temperature, and poor cycle performance make it unable to satisfy the present demand for water treatment.[9,10] Additionally, natural materials, such as clays and zeolites, have received attention as eco-friendly and economical absorbents, but their hydrophilic structures do not allow uptake of organic pollutants.[11,12] A general way to improve their absorption performance is chemical modification, but the composite's performance highly depends on the grafted or intercalated organic groups, and the modification reactions are usually complicated and may bring second time pollution.[13,14] Recently, heterostructures, integrating desired components and morphology, have already brought many unexpected discoveries in catalyst and optoelectronic devices by tuning the properties of materials and interface status.[15−17] However, the application of heterostructures for water treatment has still not been reported. Interestingly, the depletion layer of the metal semiconductor interfaces may generate electron interaction with the pollutant. Moreover, the design of inorganic heterostructures could obtain high electron mobility; thus, fast absorption rates could be expected. Therefore, heterostructure design is a promising strategy for advancing the water purification process.

Here, we first report a well-designed Ni−La_2O_3 (NLO) heterojunction structure synthesized by an electrospinning method with a remarkable ultrafast absorption rate and recyclable absorptive ability. This performance applies to various micropollutants of different molecular size and functionality that spans in agriculture, medicine, and industry fields. We speculate that the space charge layer formed at the heterointerface would endow the composite fibers excellent adsorption capacity. Moreover, the NLO nanocomposite fibers

Received: October 1, 2018
Accepted: November 26, 2018
Published: November 26, 2018

DOI: 10.1021/acsami.8b17114
ACS Appl. Mater. Interfaces 2018, 10, 43723−43729

show >97% inactivation of *Escherichia coli* in 100 min, exhibiting a rapid and thoroughly water disinfection performance. We expect that such a heterogeneous nanocomposite may have wide applications in water purification processes.

2. MATERIALS AND METHODS

2.1. Chemicals and Materials. $La(NO_3)_3{\cdot}nH_2O$, $Ni(NO_3)_2{\cdot}6H_2O$, Bisphenol A, and Bisphenol S were purchased from Sinopharm Chemical Reagent Co Ltd. Polyvinylpyrrolidone (PVP M_n 1300000) and Norit ROW 0.8 activated carbon pellets (NAC) were purchased from Alfa Aesar (China) Chemical Co., Ltd. Metolachlor was obtained from a commercial source. Ethinyl oestradiol was purchased from Aladdin Biochemical Technology Co., Ltd. All chemical reagents were used without further purification.

2.2. Synthesis of Ni–La_2O_3 Nanofibers. In a typical electrospinning procedure,[15,18] the precursor solution was prepared by dissolving nickel nitrate and lanthanum nitrate in the mixture of absolute ethanol and deionized water (1:1, volume rate). The nickel contents in NLO nanofibers were adjusted as 0, 5, 5.5, 7, and 30 at. %. Then, polyvinylpyrrolidone (PVP, M_n 1300000) was added to control the viscosity of the precursor solution. After vigorous stirring for 4 h, a homogeneous transparent solution was obtained and transferred to a stainless steel needle. Under proper high voltage and electrode distance, the precursor solution jetted accelerated from the cathode and formed a nonwoven mat at a grounded aluminum foil. The precursor nanofibers were then sintered under a nitrogen atmospheres in a tube furnace at 850 °C for 2 h at a heating rate of 5 °C/min to obtain the NLO nanofibers according to the TG-DTA results (Figure S1).

2.3. Characterization of Ni–La_2O_3 Nanofibers. *Thermoanalysis.* The thermal treatment process was based on the thermoanalysis (thermogravimetry (TG)/differential thermal analysis (DTA)) results conducted by a STA 409 instrument (Netzsch, Germany) under protective gas (nitrogen atmosphere) at a heating rate of 5 °C/min over a temperature range of 25–1000 °C.

X-ray Diffraction. The phase constitution of the samples was analyzed by X-ray diffraction (XRD, D/Max2550, Rigaku Co., Japan; using Cu Kα radiation of 0.15418 nm). All the measurements were conducted at room temperature in the range of 2θ between 20° and 50°.

SEM and TEM. Scanning electron microscopy (SEM, Merlin VP compact, Carl Zeiss, Germany) was used to characterize the morphology of the obtained nanofibers. TEM images and EDS elemental mapping were performed with a JEOL-2010F transmission electron microscope with an acceleration voltage of 200 kV.

X-ray Photoelectron Spectroscopy. The elemental and chemical states of Ni, La, and O in the composite fibers were analyzed by X-ray photoelectron spectroscopy (XPS, ESCALAB 250Xi, Thermo Fisher). A monochromatic Al Kα X-ray source and a pass energy of 30 eV were used in all samples (500 μm spot size).

FT-IR Spectroscopy. Fourier transform infrared spectroscopy was recorded by using a Vertex 70v (Bruker, Germany) at room temerprature. The sample pellets were prepared by mixing with spectroscopic grade KBr and pressing as recommended procedure in a die assembly.

Zeta Potential. The zeta potentials were measured by a Nano ZS90 (Malvern, United Kingdom) and its software (Dispersion Technology Software).

BET Surface. Surface area measurements were recorded on an Autosorb-iQ2-MP (Quantachrome Instruments U.S.). Each sample (50 mg) was degassed at 300 °C for 6 h and then filled with ultrahigh-purity nitrogen. N_2 isotherms were conducted at 77 K in a liquid nitrogen bath, and surface parameters were calculated by the Brunauer–Emmett–Teller (BET) model in the instrument software (ASiQwin).

UV–Vis Spectroscopy. Ultraviolet–visible diffuse reflectance (UV–vis) spectroscopy was performed on a UV3600 (Shimadzu, Tokyo, Japan) and recorded over 200–600 nm at room temperature.

2.4. Absorption Kinetic Studies. All absorption kinetic studies were performed at room temperature and atmospheric pressure in 30 mL liquid scintillation vials under magnetic stirring. The Ni/La_2O_3 nanofibers or La_2O_3 nanofibers were dispersed in various contaminant stock solutions (0.1 mM for each solution, 0.04 mM for ethinyl oestradiol, which has a low water solubility) with an absorbent loading of 1 g L^{-1}. Then, the mixture was continuously stirred, and 1 mL aliquots of the suspension were taken by syringe at certain intervals and immediately filtered by a 0.22 μm syringe membrane filter. The residual concentration of each pollution was determined by UV–vis spectroscopy and normalized by their measured molar extinction coefficients (BPA: 3100 at λ_{max} = 276 nm; BPS: 17950 at λ_{max} = 259 nm; metolachlor: 14400 at λ_{max} = 213 nm; and ethinyl oestradiol: 2550 at λ_{max} = 220 nm).

2.5. Flow-Through Experiment. Five milligrams of the NLO nanofibers was dispersed in 5 mL of deionized water, and then the suspension was pushed by a syringe through a 0.22 μm membrane filter. The NLO nanofibers formed a thin layer on the filter membrane. Three milliliters of a micropollutant solution (0.1 mM) was rapidly passed though the absorbent layer by a syringe in 20 s at a flow rate of 9 mL min^{-1}. The residual micropollutants in the filtrate were analyzed by UV–vis spectroscopy.

2.6. Antibacterial Test. Bacteria (*E. coli* O:H157) were cultured overnight to log phase at 37 °C in Luria–Bertani (LB) medium, collected by centrifugation, washed with physiological saline (0.9 wt % NaCl in water) to remove the nutrient from the LB medium, and diluted to ~10^5 CFU mL^{-1}. 0.5 mL of NLO solution (1 g L^{-1}) was mixed with 2 mL of the bacteria solution in a 4 mL centrifuge tube. The mixture was cultivated at 37 °C with shaking. The bacterial concentrations, which represent the disinfection efficiency, were measured at different cultivation times via a standard spread-plating technique. Ten microliters of the suspension was removed at certain intervals, spread in triplicate onto the LB medium after a 10× dilution and incubated at 37 °C for 24 h. The bacterial growth curve was obtained by incubating the bacterial solution without the addition of NLO nanofibers for 5 days.

2.7. Regeneration of Ni–La_2O_3 Nanofibers. Four milligrams of NLO nanofibers was transferred into a 5 mL Eppendorf tube, and four mL (0.1 mM) of a BPA solution was added. After shaking for 5 min, the mixture was centrifuged to separate the solution and nanofibers. The residual BPA in the solution was measured by UV–vis spectroscopy. The NLO nanofibers were regenerated by methanol wash. The absorption and desorption processes were performed five times to test the reusability and stability of the NLO nanofibers.

3. RESULTS AND DISCUSSION

The NLO heterostructure nanofibers were fabricated via electrospinning and followed by a proper annealing process (Figure S1). This methodology for preparing flexible and uniform heterostructure fibers is based on our previous study.[15,18] The morphology of NLO nanofibers has been evidenced by scanning electron microscopy (SEM) and transmission electron microscopy (TEM) (Figure 1 and Figure S2). The continuous nanofibers had smooth surface and flexible structure. TEM was also used to observe the distribution of Ni particles in the La_2O_3 matrix, shown in Figure 1. The high-resolution transmission electron spectroscopy (HRTEM) image of the selected area corresponding to the interface of nickel and lanthanum oxide is presented in Figure 1a. Lattice spacings of 2.08 and 3.07 Å can be indexed to the (111) plane of metallic Ni and (002) plane of La_2O_3, directly confirming its metal–semiconductor heterogeneous structure. A selected-area electron diffraction (SAED) pattern of the NLO nanofibers (inset of Figure 1a) could be indexed as polycrystalline La_2O_3. Ultrathin cross-sectioning and TEM images with energy-dispersive X-ray spectroscopy (EDS) clearly show the perfect fiber morphology and homogeneous

DOI: 10.1021/acsami.8b17114
ACS Appl. Mater. Interfaces 2018, 10, 43723–43729

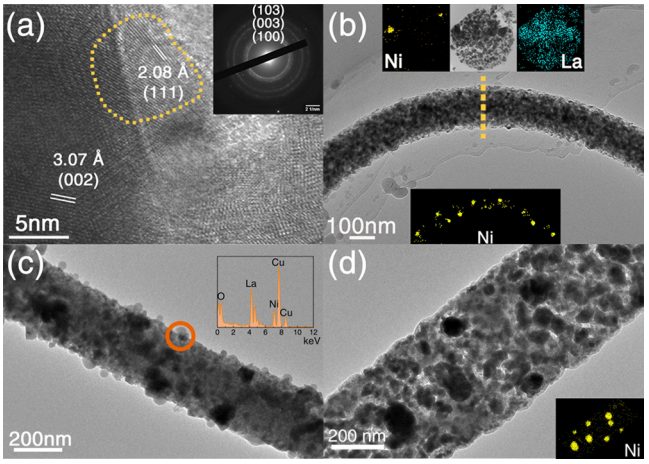

Figure 1. TEM image of Ni–La_2O_3 nanofibers with various Ni contents. (a) HRTEM image of Ni and La_2O_3 interface. Inset: a selected area electron diffraction pattern. (b) TEM images of a 5.5 at. % Ni–La_2O_3 nanofiber (inset: EDS mapping of Ni element along the nanofiber and in cross section). (c) Ni-7 at. % (insets: typical EDS microanalysis on selected areas of a single nanowire). (d) Ni-30 at. % (inset: EDS mapping of Ni element along the nanowire).

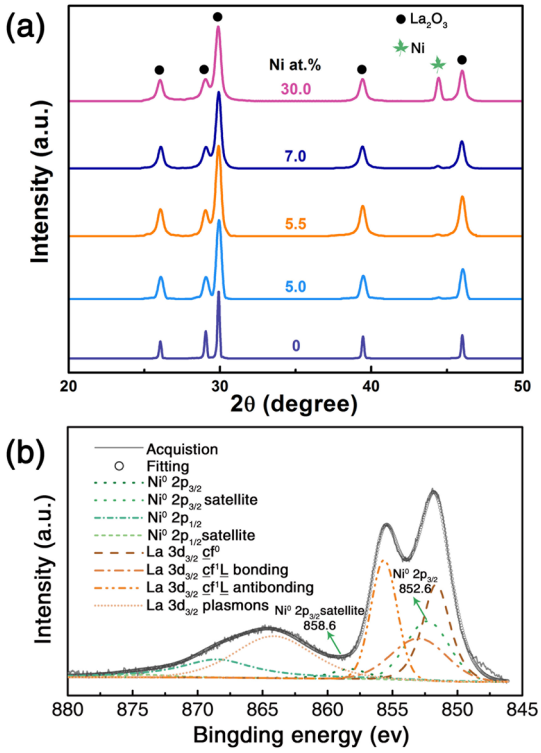

Figure 2. (a) XRD patterns of NLO nanofibers with various Ni contents. (b) Ni 2p XPS spectrum of the NLO nanofibers (5.5 at. % Ni).

dispersion of Ni particles ~10 nm in size of the 5.5 at. % Ni–La_2O_3 nanofibers (Figure 1b). Figure 1c reveals the grain growth of specific Ni particles (black spots) in 7 at. % Ni–La_2O_3 nanofibers, and the EDS result demonstrates the composition of NLO nanofibers, including Ni and La. Further increase of the Ni content (30 at. %) could induce the abnormal grain growth and aggregation of Ni particles, as shown in Figure 1d.

Furthermore, the phase composition and structure of the as-synthesized NLO nanofibers were examined by X-ray diffraction (Figure 2a). All of the reflection peaks can be indexed to hexagonal La_2O_3 and cubic Ni. No impurity phase like NiO was observed. To clarify the elemental and chemical state of Ni in the NLO heterostructure nanofibers, high-resolution X-ray photoelectron spectra (XPS) were introduced (Figure 2b and Figure S3). Although the peak of Ni 2p overlapped with La 3d, it is still possible to distinguish them by fine peak fitting. As shown in Figure 2b, the Ni $2p_{3/2}$ peak appears at 852.6 eV with satellite 6.0 eV above the main peak, indicating the metallic nature of nickel.[19,20] No impurity peak of Ni $^{2+}$ appeared around 857.9 eV.

The absorptive properties of NLO nanofibers were systematically evaluated by using bisphenol A (BPA), which is a harmful EDC to living organisms even at low concentrations, as a model pollutant and compared with those of commercial Norit 0.8 activated carbon (NAC).[21] Figure 3a shows the influence of the Ni content on the absorption efficiency. Pure La_2O_3 nanofibers show a poor absorption ability, which is ascribed to its well-known deliquesce property. After the introduction of Ni, a substantial increase in the absorptive efficiency is observed, reaching the optimum value at 5.5 at. % and then decreasing. This deterioration may be due to Ni aggregation reducing the active sites on the interface (Figure 1d).

As shown in Figure 3b, the NLO nanofibers removed 89% of BPA in 10 s, reaching 92% of its equilibrium uptake. Meanwhile, NAC showed only 7% of its equilibrium uptake in 10 s and required more than 10 min to reach equilibrium.

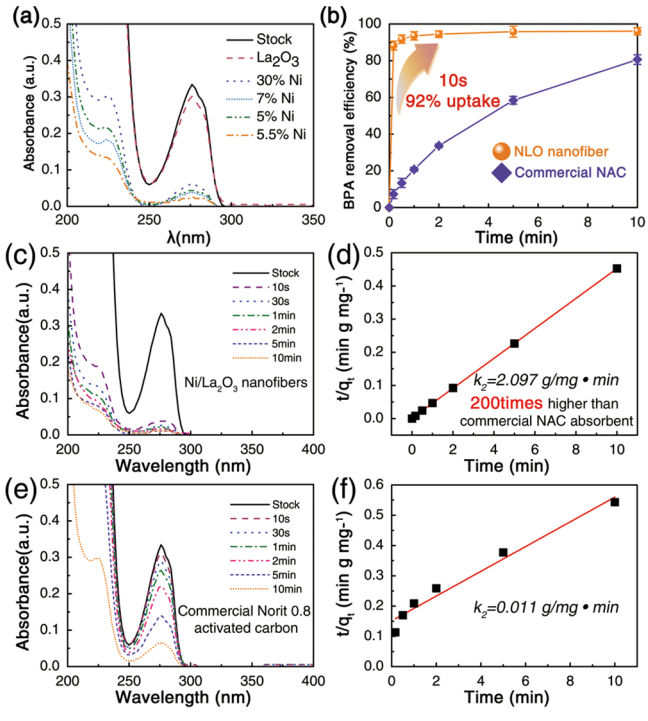

Figure 3. BPA uptake rate of NLO nanofibers compared with commercial Norit 0.8 activated carbon powders. (a) Bisphenol A (0.1 mM) uptake by pure La_2O_3 and NLO nanofibers with different Ni contents. (b) BPA removal efficiency of NLO nanofibers and commercial NAC powder (1 mg mL^{-1}). (c–f) Time-dependent absorption of BPA recorded by UV–vis spectra and pseudo-second-order absorption kinetics plots for NLO (c, d) and NAC (e, f), respectively.

DOI: 10.1021/acsami.8b17114
ACS Appl. Mater. Interfaces 2018, 10, 43723–43729

The absorption process can be considered a pseudo-second-order reaction, and its kinetics can be expressed as

$$\frac{t}{q_t} = \frac{t}{k_2 q_e^{\ 2}} + \frac{1}{q_e} \quad (1)$$

where q_e and q_t are the contaminant amounts absorbed on the NLO nanofibers at equilibrium and at time t (mg g^{-1}), respectively, and k_2 is the pseudo-second-order rate constant (g mg^{-1} min^{-1}). The BPA uptake rate constant of NLO is 2.097 g mg^{-1} min^{-1}, which is 200 times higher than that of NAC (Figure 3)[22] and orders of magnitude higher than other studied absorbents (Figure 4). To our knowledge, the rate

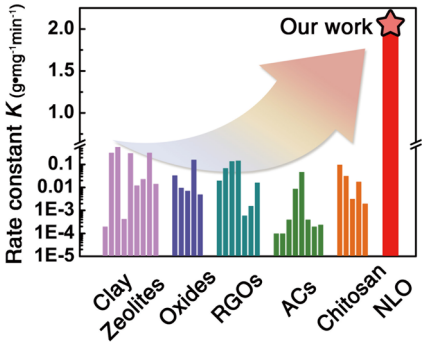

Figure 4. Absorption performance of NLO nanofibers compared with various absorbents.

constant in our work is the highest reported for BPA or other micropollutants uptake by zeolites or chemically modified natural materials, carbon and graphene based absorbents, oxides and nanocomposites, activated carbons, and chitosan under the similar experimental conditions, demonstrating that the NLO nanofibers meet the demand for an instant water purification technique.[11−13,23−31]

Compared with the energy-intensive and degradative regeneration process of activated carbon, NLO nanofibers can be regenerated by a soft methanol wash process at room temperature with no obvious performance decay after five absorption and desorption cycles (Figure 5). The nanofibers can also be easily separated during the regenerative process because of their fibrous morphology, which prevents secondary pollution caused by small powder absorbents leaking. As shown in the inset of Figure 5, the NLO composite maintains its fibrous structure after five cyclic tests, which ensures the

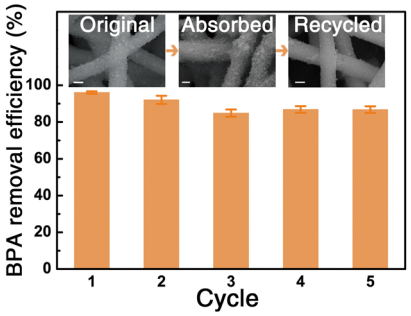

Figure 5. BPA removal efficiency by NLO nanofibers in sequential regeneration cycles. Inset: SEM images of NLO nanofibers (Ni content 5.5 at. %): original, after absorption and recycled (scale bar: 200 nm).

NLO nanofibers stability. Moreover, as portable water treatment products or water-purification units, the NLO nanofibers are economically comparable with commercial activated carbon filters, which generally cannot be recycled and have to be replaced after purifying ∼200 L of water.

Furthermore, in addition to BPA, we selected other representative EDCs of different functionality and size that commonly found in wastewater to test the performance of the NLO nanofibers (inset of Figure 6a).[32−35] Among these, BPS

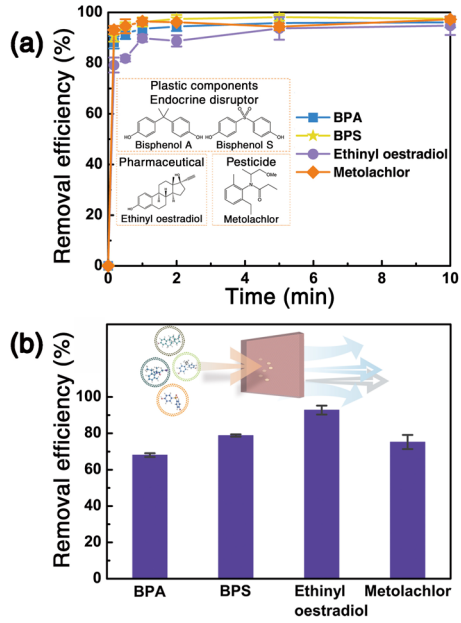

Figure 6. (a) Time-dependent absorptive efficiency of various micropollutants. Inset: structures and classification of the tested pernicious micropollutants. (b) Removal of each micropollutant under rapid flow-through condition. Inset: sketch of the flow-through test.

has been widely used in the production of polycarbonate, epoxy resins, and phenolic resins as a substitute of BPA; however, it is also proven to be harmful to the endocrine system. Ethinyl oestradiol, a major ingredient in birth-control pills, can lead to the extinction of wild fish population at low concentration (5−6 ng L^{-1}). Metolachlor is a popular preemergence herbicide that has been widely detected in groundwater and surface water. As shown in Figure 6a and Figure S4, the NLO nanofibers can rapidly remove these micropollutants, including detrimental plastic components, pesticides, and pharmaceuticals, with high absorption rates (Table S1) and reach equilibrium in 5 min, showing broad application prospects.

To make the NLO absorbent more compatible with current portable water purification devices, we designed a fluid experiment to simulate an application environment which challenges the general laboratory test results. As illustrated in the inset of Figure 6b, each pollution solution was rapidly passed through a thin layer of the NLO nanofibers at an 8−9 mL min^{-1} flow rate. Under this rigorous condition, the NLO nanofibers still had a strong absorption behavior and removed 80% BPS, 79% metolachlor, 68% BPA, and 95% ethinyl oestradiol, indicating their high potential for practical applications.

DOI: 10.1021/acsami.8b17114
ACS Appl. Mater. Interfaces 2018, 10, 43723−43729

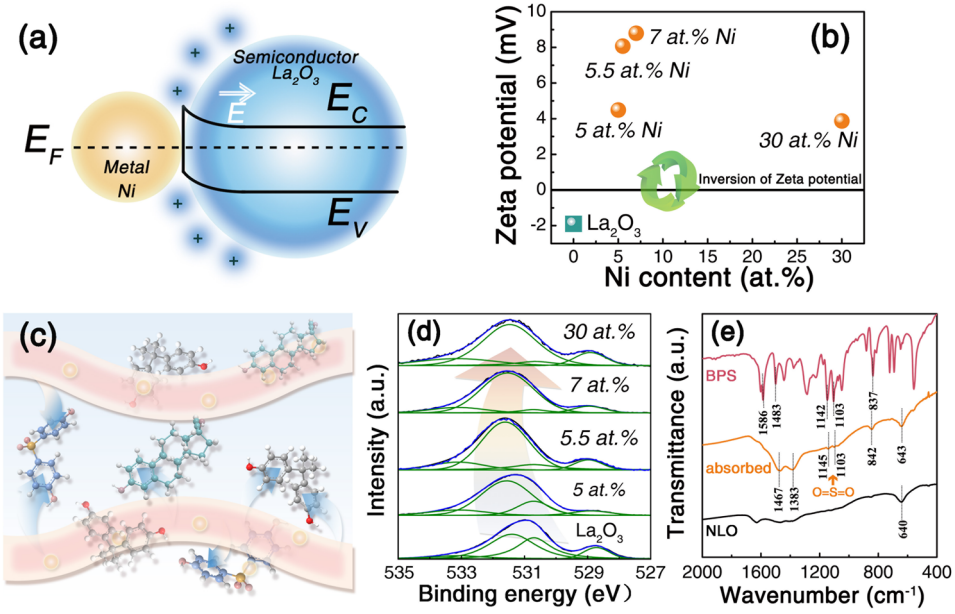

Figure 7. (a) Diagrammatic sketch of the Ni–La_2O_3 heterojunction. (b) Zeta potential of pure La_2O_3 and NLO nanofibers with different Ni content. (c) Schematic of the absorption mechanism. (d) O 1s XPS spectrum of the NLO nanofibers. (e) FTIR spectra of NLO nanofibers, NLO nanofibers after BPS absorption, and BPS.

The fast and versatile adsorption characteristics of the nanofibers can be attributed to their special heterojunction structure, which is well-known in catalysis and photoelectronics but has not been reported for adsorption applications.[36,37] The Ni–La_2O_3 composite has a typical metal oxide heterogeneous band structure.[38] Nickel has a larger work function than La_2O_3,[39] and when Ni is in contact with lanthanum oxide, electrons will flow from La_2O_3 to Ni to equalize the Fermi energy levels. This charge transfer will leave behind a uniform, positive space charge layer in the depletion region on the La_2O_3 surface where the bands will bend upward (Figure 7a) and simultaneously tune the surface charge state, as observed in the zeta potential test (Figure 7b). This positive charge layer will further promote the absorption process by attracting and sharing electrons with electron-rich organic groups,[40] such as benzene rings, on micropollutants, making NLO nanofibers widely applicable for various organic pollutants, as illustrated in Figure 7c. Meanwhile, by introducing proper and well-distributed Ni nanoparticles into the La_2O_3 host, the areas of the heterogeneous interface and positive space charge layer are maximized, which is critical for an ultrafast absorption efficiency (Figure 3a). The large BET surface area of the NLO nanofibers (S_{BET} = 143 m^2 g^{-1}) also contributes to rapid micropollutants removal (Figure S5). Furthermore, integrating the fiber flexibility and excellent mechanical properties of the inorganic composite material ensures the reusability of NLO nanofibers (Figure S2).

To gain more insight, XPS and FTIR studies were performed. Figure 7d shows the XPS O 1s spectra of the NLO nanofibers. The shift in the bonding energy to higher values indicates the electron transfer process from La_2O_3 to Ni and the formation of heterogeneous interface,[41] which coincides with our mechanism deduction. The FTIR spectra of each contaminant and the NLO nanofibers before and after absorbing the contaminants are presented in Figure 7e and Figure S6. Clearly, many new peaks, which matched the characteristic peaks of the contaminants, such as the O=S=O group of BPS at 1140 cm^{-1}, were observed in the NLO spectra after the absorption process, demonstrating that the micropollutants were absorbed on the surface of the NLO nanofibers (Figure 7e). After absorption, the red-shift of the C=C characteristic peak indicates an electron interaction between the benzene ring and the space charge region on the NLO nanofibers, which is also in good agreement with the proposed mechanism.

In addition to the above-mentioned excellent absorptive properties, NLO nanofibers are versatile water treatment materials with excellent bactericidal ability. Here, we chose *Escherichia coli* O157,[5] a global health concern, to evaluate this ability. The NLO nanofibers showed a high germicidal efficacy, i.e., ~97% inactivation, for a bacterial concentration as high as 10^8 CFU L^{-1} in 100 min with a very small quantity of NLO nanofibers (200 mg L^{-1}), as shown in Figure 8. No *E. coli* recovery was detected after 1 day, while the blank control had proliferation of 3 orders of magnitude (inset of Figure 8). The

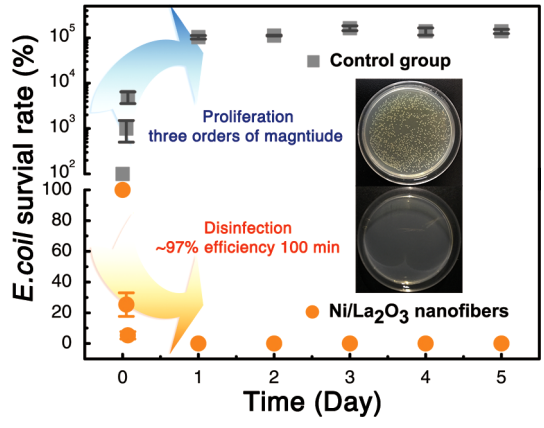

Figure 8. Bactericidal property. *E. coli* survival status with and without NLO nanofibers treatment. Inset: optical images of *E. coli* growth results after 1 day cultivation.

DOI: 10.1021/acsami.8b17114
ACS Appl. Mater. Interfaces 2018, 10, 43723–43729

NLO nanofibers exhibit a faster and more thorough disinfection efficiency than most reported synthetic polycationic polymers, photocatalysts, and other nanocomposite materials,[42,43] demonstrating their application prospects for enhancing water quality. This remarkable antimicrobial ability is also due to the positive space region formed after a proper Ni addition, which facilitates the electrostatic interactions between the NLO nanofibers and net negative charges on the bacterial outer cell membrane due to anionic phospholipids and the phosphate groups on lipopolysaccharides. These interactions will result in a permeability change in the bacterial cell wall. Subsequently, ion channels, transmembrane pores, and extensive membrane ruptures will be caused by nanofibers insertion. Finally, microbial cell lysis and cytoplasmic content leakage will lead to cell death,[44] as shown in Figure S7.

4. CONCLUSION

In summary, NLO nanocomposites with designed heterogeneous structures have been fabricated by the simple electrospinning method. The as-synthesized NLO nanofibers have a polycrystalline La_2O_3 matrix with homogeneous dispersion of Ni particles ~10 nm in size. This metal−semiconductor heterostructure is applied to obtain superior absorption performance for the first time. It exhibits ultrafast uptake of various micropollutants, >92% in the first 10 s, with the highest absorption rate constant. Moreover, the NLO nanofibers can be regenerated several times by a soft methane wash process maintaining stable performance, which is economically competitive. Finally, the microbe sterilization ability widely broadens the application scope of the NLO nanocomposites. It is expected that the NLO nanocomposites could be useful for ensuring drinking water quality and relieving the worldwide water shortage, also providing a new idea for designing high-efficiency absorbent materials.

■ ASSOCIATED CONTENT

Supporting Information

The Supporting Information is available free of charge on the ACS Publications website at DOI: 10.1021/acsami.8b17114.

TG-DTA results, SEM images of NLO nanofibers, XPS, BET surface area, FTIR and UV−vis characterization (PDF)

■ AUTHOR INFORMATION

Corresponding Author

*E-mail: panw@mail.tsinghua.edu.cn (W.P.).

ORCID

Yan Xing: 0000-0002-7210-2458

Meng Zhao: 0000-0003-1002-7998

Notes

The authors declare no competing financial interest.

■ ACKNOWLEDGMENTS

We gratefully acknowledge the support of the National Natural Science Foundation of China (Grant 51323001).

■ REFERENCES

(1) Oki, T.; Kanae, S. Global Hydrological Cycles and World Water Resources. *Science* **2006**, *313*, 1068−1072.

(2) Organization, W. H. *Guidelines for Drinking Water Quality*, 4th ed.; World Health Organization: Geneva, 2011.

(3) Richardson, S. D. Water Analysis: Emerging Contaminants and Current Issues. *Anal. Chem.* **2009**, *81*, 4645−4677.

(4) Schwarzenbach, R. P.; Escher, B. I.; Fenner, K.; Hofstetter, T. B.; Johnson, C. A.; Von Gunten, U.; Wehrli, B. The Challenge of Micropollutants in Aquatic Systems. *Science* **2006**, *313*, 1072−1077.

(5) Mead, P. S.; Griffin, P. M. Escherichia Coli o157: H7. *Lancet* **1998**, *352*, 1207−1212.

(6) Diamanti-Kandarakis, E.; Bourguignon, J. P.; Giudice, L. C.; Hauser, R.; Prins, G. S.; Soto, A. M.; Zoeller, R. T.; Gore, A. C. Endocrine-Disrupting Chemicals: An Endocrine Society Scientific Statement. *Endocr. Rev.* **2009**, *30*, 293−342.

(7) Vandenberg, L. N.; Hauser, R.; Marcus, M.; Olea, N.; Welshons, W. V. Human Exposure to Bisphenol A (BPA). *Reprod. Toxicol.* **2007**, *24*, 139−177.

(8) Gupta, V. K.; Ali, I.; Saleh, T. A.; Nayak, A.; Agarwal, S. Chemical Treatment Technologies for Waste-Water Recycling—An Overview. *RSC Adv.* **2012**, *2*, 6380−6388.

(9) Órfão, J.; Silva, A.; Pereira, J.; Barata, S.; Fonseca, I.; Faria, P.; Pereira, M. Adsorption of a Reactive Dye on Chemically Modified Activated Carbons−Influence of pH. *J. Colloid Interface Sci.* **2006**, *296*, 480−489.

(10) San Miguel, G.; Lambert, S.; Graham, N. The Regeneration of Field-Spent Granular-Activated Carbons. *Water Res.* **2001**, *35*, 2740−2748.

(11) Bhatnagar, A.; Sillanpää, M. Utilization of Agro-Industrial and Municipal Waste Materials as Potential Adsorbents for Water Treatment—A Review. *Chem. Eng. J.* **2010**, *157*, 277−296.

(12) Putra, E. K.; Pranowo, R.; Sunarso, J.; Indraswati, N.; Ismadji, S. Performance of Activated Carbon and Bentonite for Adsorption of Amoxicillin from Wastewater: Mechanisms, Isotherms and Kinetics. *Water Res.* **2009**, *43*, 2419−2430.

(13) Park, Y.; Sun, Z.; Ayoko, G. A.; Frost, R. L. Bisphenol A Sorption by Organo-Montmorillonite: Implications for the Removal of Organic Contaminants from Water. *Chemosphere* **2014**, *107*, 249−256.

(14) Cao, F.; Bai, P.; Li, H.; Ma, Y.; Deng, X.; Zhao, C. Preparation of Polyethersulfone-Organophilic Montmorillonite Hybrid Particles for the Removal of Bisphenol A. *J. Hazard. Mater.* **2009**, *162*, 791−798.

(15) Lin, D.; Wu, H.; Zhang, R.; Pan, W. Enhanced Photocatalysis of Electrospun Ag−ZnO Heterostructured Nanofibers. *Chem. Mater.* **2009**, *21*, 3479−3484.

(16) Duan, J.; Chen, S.; Chambers, B. A.; Andersson, G. G.; Qiao, S. Z. 3D WS_2 Nanolayers@Heteroatom-Doped Graphene Films as Hydrogen Evolution Catalyst Electrodes. *Adv. Mater.* **2015**, *27*, 4234−4241.

(17) Cai, Z.; Liu, B.; Zou, X.; Cheng, H. M. Chemical Vapor Deposition Growth and Applications of Two-Dimensional Materials and Their Heterostructures. *Chem. Rev.* **2018**, *118*, 6091−6133.

(18) Wu, H.; Sun, Y.; Lin, D.; Zhang, R.; Zhang, C.; Pan, W. GaN Nanofibers based on Electrospinning: Facile Synthesis, Controlled Assembly, Precise Doping, and Application as High Performance UV Photodetector. *Adv. Mater.* **2009**, *21*, 227−231.

(19) Grosvenor, A. P.; Biesinger, M. C.; Smart, R. St.C.; McIntyre, N. S. New Interpretations of XPS Spectra of Nickel Metal and Oxides. *Surf. Sci.* **2006**, *600*, 1771−1779.

(20) Sunding, M. F.; Hadidi, K.; Diplas, S.; Løvvik, O. M.; Norby, T. E.; Gunnæs, A. E. XPS Characterisation of In Situ Treated Lanthanum Oxide and Hydroxide Using Tailored Charge Referencing and Peak Fitting Procedures. *J. Electron Spectrosc. Relat. Phenom.* **2011**, *184*, 399−409.

(21) Rochester, J. R. Bisphenol A and Human Health: A Review of the Literature. *Reprod. Toxicol.* **2013**, *42*, 132−155.

(22) Ho, Y. S. Review of Second-Order Models for Adsorption Systems. *J. Hazard. Mater.* **2006**, *136*, 681−689.

(23) Bhatnagar, A.; Anastopoulos, I. Adsorptive Removal of Bisphenol A (BPA) from Aqueous Solution: A review. *Chemosphere* **2017**, *168*, 885−902.

DOI: 10.1021/acsami.8b17114
ACS Appl. Mater. Interfaces 2018, 10, 43723−43729

(24) Ortiz Martínez, K.; Reddy, P.; Cabrera Lafaurie, W. A.; Román, F. R.; Hernández Maldonado, A. J. Single and Multi-Component Adsorptive Removal of Bisphenol A and 2, 4-Dichlorophenol from Aqueous Solutions with Transition Metal Modified Inorganic−Organic Pillared Clay Composites: Effect of pH and Presence of Humic Acid. *J. Hazard. Mater.* **2016**, *312*, 262−271.
(25) Alsbaiee, A.; Smith, B. J.; Xiao, L.; Ling, Y.; Helbling, D. E.; Dichtel, W. R. Rapid Removal of Organic Micropollutants from Water by A Porous *β*-Cyclodextrin Polymer. *Nature* **2016**, *529*, 190−195.
(26) Tsai, W. T.; Lai, C. W.; Su, T. Y. Adsorption of Bisphenol-A from Aqueous Solution onto Minerals and Carbon Adsorbents. *J. Hazard. Mater.* **2006**, *134*, 169−175.
(27) Hasan, M.; Ahmad, A.; Hameed, B. Adsorption of Reactive Dye onto Cross-Linked Chitosan/Oil Palm Ash Composite Bbeads. *Chem. Eng. J.* **2008**, *136*, 164−172.
(28) Peng, S.; Hao, K.; Han, F.; Tang, Z.; Niu, B.; Zhang, X.; Wang, Z.; Hong, S. Enhanced Removal of Bisphenol-AF onto Chitosan-Modified Zeolite by Sodium Cholate in Aqueous Solutions. *Carbohydr. Polym.* **2015**, *130*, 364−371.
(29) Jin, Z.; Wang, X.; Sun, Y.; Ai, Y.; Wang, X. Adsorption of 4-n-Nonylphenol and Bisphenol-A on Magnetic Reduced Graphene Oxides: A Combined Experimental and Theoretical Studies. *Environ. Sci. Technol.* **2015**, *49*, 9168−9175.
(30) Chen, Y.; Chen, L.; Bai, H.; Li, L. Graphene Oxide−Chitosan Composite Hydrogels as Broad-Spectrum Adsorbents for Water Purification. *J. Mater. Chem. A* **2013**, *1*, 1992−2001.
(31) Libbrecht, W.; Vandaele, K.; De Buysser, K.; Verberckmoes, A.; Thybaut, J. W.; Poelman, H.; De Clercq, J.; Van Der Voort, P. Tuning the Pore Geometry of Ordered Mesoporous Carbons for Enhanced Adsorption of Bisphenol-A. *Materials* **2015**, *8*, 1652−1665.
(32) Viñas, R.; Watson, C. S. Bisphenol S Disrupts Estradiol-Induced Nongenomic Signaling in a Rat Pituitary Cell Line: Effects on Cell Functions. *Environ. Health Perspect.* **2013**, *121*, 352−358.
(33) Kidd, K. A.; Blanchfield, P. J.; Mills, K. H.; Palace, V. P.; Evans, R. E.; Lazorchak, J. M.; Flick, R. W. Collapse of a Fish Population after Exposure to a Synthetic Estrogen. *Proc. Natl. Acad. Sci. U. S. A.* **2007**, *104*, 8897−8901.
(34) Miege, C.; Choubert, J.; Ribeiro, L.; Eusèbe, M.; Coquery, M. Fate of Pharmaceuticals and Personal Care Products in Wastewater Treatment Plants−Conception of a Database and First Results. *Environ. Pollut.* **2009**, *157*, 1721−1726.
(35) Falconer, I. R.; Chapman, H. F.; Moore, M. R.; Ranmuthugala, G. Endocrine−Disrupting Compounds: A Review of Their Challenge to Sustainable and Safe Water Supply and Water Reuse. *Environ. Toxicol.* **2006**, *21*, 181−191.
(36) Kudo, A.; Miseki, Y. Heterogeneous Photocatalyst Materials for Water Splitting. *Chem. Soc. Rev.* **2009**, *38*, 253−278.
(37) Li, D.; Xia, Y. Electrospinning of Nanofibers: Reinventing the Wheel? *Adv. Mater.* **2004**, *16*, 1151−1170.
(38) Rhoderick, E. H. Metal-Semiconductor Contacts. *IEE Proc., Part I: Solid-State Electron Devices* **1982**, *129*, 1−14.
(39) Wei, C.; Ren, Q. Q.; Fan, J. L.; Gong, H. R. Cohesion Properties of W/La_2O_3 Interfaces from First Principles Calculation. *J. Nucl. Mater.* **2015**, *466*, 234−238.
(40) Timmer, A.; Monig, H.; Uphoff, M.; Diaz Arado, O.; Amirjalayer, S.; Fuchs, H. Site-Specific Adsorption of Aromatic Molecules on a Metal/Metal Oxide Phase Boundary. *Nano Lett.* **2018**, *18*, 4123−4129.
(41) Sutthiumporn, K.; Kawi, S. Promotional Effect of Alkaline Earth Over Ni−La_2O_3 Catalyst for CO_2 Reforming of CH_4: Role of Surface Oxygen Species on H_2 Production and Carbon Suppression. *Int. J. Hydrogen Energy* **2011**, *36*, 14435−14446.
(42) Malato, S.; Fernández Ibáñez, P.; Maldonado, M. I.; Blanco, J.; Gernjak, W. Decontamination and Disinfection of Water by Solar Photocatalysis: Recent Overview and Trends. *Catal. Today* **2009**, *147*, 1−59.
(43) Irwansyah, I.; Li, Y. Q.; Shi, W.; Qi, D.; Leow, W. R.; Tang, M. B.; Li, S.; Chen, X. Gram−Positive Antimicrobial Activity of Amino Acid−Based Hydrogels. *Adv. Mater.* **2015**, *27*, 648−654.
(44) Brogden, K. A. Antimicrobial Peptides: Pore Formers or Metabolic Inhibitors in Bacteria? *Nat. Rev. Microbiol.* **2005**, *3*, 238−250.

DOI: 10.1021/acsami.8b17114
ACS Appl. Mater. Interfaces 2018, 10, 43723−43729